Channel Adapted Antenna Augmentation for Improved Wi-Fi Throughput

Yanbo Zhang, Weiping Sun, Yidong Ren, Sung-ju Lee, *Fellow, IEEE,* and Mo Li, *Fellow, IEEE*

Abstract—This paper investigates how the expansion of array size may improve the spatial diversity of state-of-the-art Wi-Fi system and increase its throughput. With comprehensive Wi-Fi measurement studies with augmented antennas, we identify the potential performance gain atop spatial diversity gains from existing technologies like MIMO and beamforming. We propose WINAS, a general Wi-Fi intelligent antenna selection scheme with full system implementation that can be easily integrated with commodity Wi-Fi AP. WINAS provides substantially improved throughput for downlink traffics. Our experimental evaluation suggests that WINAS improves Wi-Fi throughput up to 1.56x, and 1.47x in average, in real user-based evaluation.

Index Terms—Wireless system, communication, measurement, channel adaptation, antenna augmentation, Wi-Fi throughput

1 Introduction

High throughput has been a paramount concern of Wi-Fi for supporting Gigabit Internet. The maximum physical data rate (PHY-rate) defined in 802.11ac is up to 6.933 Gbps [1]. In practical usage, however, the true data rate is fundamentally limited by the quality of the wireless channel that the radio signal experiences. If the wireless channel quality is not favourable, Wi-Fi transmission has to fall back to lower-order modulation and higher coding redundancy in order to cope with a low signal-to-noise ratio (SNR) [2], [3], [4]. The 802.11ac application data rate has been reported to be at the order of 90 to 200 Mbps at different locations in a typical office environment [5], [6].

Previous Wi-Fi editions have employed schemes such like MIMO (since 802.11n, MU-MIMO of 802.11ac/ax) and beamforming (since 802.11ac) to improve the data rate by leveraging space — the wireless channel varies across different Tx/Rx pairs due to multipath propagation of the signal, and thus offers opportunities for multiplexing or directional signal enhancement [7]. The adoption of MIMO and beamforming has brought significant improvement to the Wi-Fi throughput. The performance gain of MIMO and beamforming, however, is still limited by the number of Tx/Rx pairs, which has not grown much due to the hardware cost (RF chain components including LNA, mixer, LPF, ADC) and the incurred processing overhead (e.g. 20MHz sampling rate adds 40M I/Q samples per RF chain) for MMSE channel estimator[8], [9], [10] and STBC coder/decoder[11], which in turn requires more powerful processor with higher cost. To our knowledge, even the most advanced 802.11ax commercial Wi-Fi APs (e.g. ROG GT-AX11000, TL-ARCHER AX90) use utmost four RF chains for single band (2.4 GHz or 5 GHz), and are priced at above $300. ON semiconductor develops QT7810X RF transceiver [12] with up to eight radio chains for 802.11ax, which however is not available at the market.

Given the limit on the number of radio chains of Wi-Fi chipset, in this paper, we investigate how the increase of antennas in space may improve the spatial diversity gain on top of existing schemes like MIMO and beamforming. The rationale of antenna augmentation comes from the fact that multiple antennas offer multiple observations of the same signal. If one antenna is experiencing a destructive superposition of multi-path signals, it is likely that another antenna encounters the opposite situation. If a Wi-Fi device has more antennas than its radio chains, it can choose from the possible antenna combinations and use the best one to provide the highest throughput.

The concept of "antenna selection" has been studied in past literatures, but mostly in theory [13], [14], [15], [16], which proved that additional diversity gain can be obtained by selecting different sets of antennas atop fixed number of radio chains. Algorithms and methods around optimizing antenna selection have been proposed [17], [18], [19], [20], [21] and mostly assessed by simulated wireless transmissions. To the best of our knowledge, however, little systematic development and application to commodity wireless systems, e.g., Wi-Fi, has been performed mainly due to the following challenges: 1) *Low scalability.* Most existing antenna selection algorithms incur excessive channel probing overhead and are thus not practical to scale with larger size of the antenna array - the two known recent system developments by Huawei [22] and Samsung[23] are limited to two antennas per radio chain. 2) *Inadequate adaptability.* Adapting to wireless channel variation and efficiently switching to more appropriate antennas is necessary to maintain high throughput but seldomly investigated in existing literatures - significant system design consideration

- *Y. Zhang and M. Li are with the School of Computer Science and Engineering, Nanyang Technological University, Singapore 639798. E-mail: yanbo001@e.ntu.edu.sg, limo@ntu.edu.sg*
- *W. Sun is with Samsung Research and Development, 6G Research Team, Seoul, KR 06620. E-mail: wp.son@samsung.com*
- *Y. Ren is with the Department of Computer Science and Engineering, Michigan State University, East Lansing, MI 48824. Email: renyidon@msu.edu.sg*
- *S. Lee is with School of Computing, Korea Advanced Institute of Science & Technology (KAIST), Daejeon, KR 34141. Email: profsj@kaist.ac.kr*

Manuscript received January 18, 2022; firstly revised May 16, 2022; secondly revised June 28, 2022; accepted July 20, 2022.
(Corresponding author: Mo Li)

is lacking. 3) *Protocol compatibility.* No existing studies can easily generalize to typical Wi-Fi scenario where protocol compatibility has to be ensured - in order to integrate 802.11 MAC and PHY behaviors involved in channel sounding, rate adaptation, and multiple access.

This paper performs a measurement study to reveal the spatial diversity gain atop existing MIMO and beamforming technique. Our investigation shows up to 1.9x and 1.65x throughput gains atop MIMO on 2.4 GHz and 5 GHz, respectively. There is 1.2x throughput gain even when beamforming is enabled.

Following the measurement study, we propose WINAS, a general Wi-Fi INtelligent Antenna Selection scheme for antenna augmentation of commercial Wi-Fi APs. The proposed solution can be easily integrated with commodity Wi-Fi AP to augment the number of candidate antennas connected to each radio chain and improve its spatial diversity. The AP can configure the RF switches to select a combination of antennas on demand for best communication performance. The prototype we build consists of a commodity Wi-Fi AP with three radio chains and a linear antenna array with 12 antennas. All components are connected through standard hardware interfaces and work in a plug-and-play mode without any hardware modifications to the AP. The total hardware cost including antennas and RF switches is below $30 which is far lower than the cost of increasing radio chains to achieve antenna array of the same size. Fig. 1(a) shows the prototype platform. To fully exploit the augmented antennas and address aforementioned challenges in system design, WINAS entails an intelligent antenna combination (*AntComb*) control, by which the AP can quickly identify the best *AntComb*, tailoring for wireless channel condition, and achieve fast antenna switching in milliseconds. Instead of heavily probing instantaneous channel condition, WINAS predicts variation of channel quality with a machine learning based estimator, achieves timely *AntComb* switches, while at the same time avoids unnecessary probing overhead. For compatibility consideration, WINAS embeds itself into 802.11 standard MAC and PHY operations that involve light modification to 802.11 modulation and coding scheme (MCS) control, and is able to support multi-client scenarios.

End-to-end system performance is evaluated with extensive real world experiments conducted in different environmental conditions. Compared with legacy Wi-Fi, the averaged throughput gain delivered by WINAS is 1.61x and 1.47x with single client and multiple clients scenarios, respectively.

In summary, we claim the following contributions.

- To the best of our knowledge, we are the first to experimentally investigate the spatial diversity gain brought by antenna augmentation with commodity Wi-Fi.
- We develop a complete end-to-end design, enabling an intelligent utilization of the augmented antennas.
- We implement a real-time system with hardware extension and software modification compatible with commodity 802.11 AP, with which the performance of the proposed design can be corroborated by real world experiments.

The rest of this paper is organized as follows: In Section 2, we summarize and discuss the related work. In Section 3, we provide a preliminary measurement study to investigate potential gain from antenna augmentation. In Section 4, we introduce the design of WINAS. Three extended topics regarding WINAS are discussed in Section 6. The performance of WINAS is evaluated with extensive experiment results in Section 5. We conclude the paper in Section 7.

2 Related Work

Multi-antenna systems. From the first paper [24] that proves the possibility of MIMO, the major efforts in the direction of exploiting spatial diversity have been made to improve multiplexing and transmit/receive diversity, where multiple RF chains are used simultaneously to increase spatial streams, provide redundant copies, or enhance signal strength in directions [25], [26], [27]. Recent Massive MIMO [28], [29], [30] may scale up to hundreds of antennas to simultaneously serve many cells with the same time frequency resource. It is one crucial PHY technique for the 5G base stations. The increased number of RF chains in MIMO, however, imposes excessive processing overhead regarding both infrastructural and computational cost, which makes the multi-antenna systems in-affordable to wireless local area networks like those of Wi-Fi. To our knowledge, the maximum number of RF chains accommodated in single commercial Wi-Fi chipset (being 2.4 GHz or 5 GHz) is four. As our empirical study suggests, WINAS can provide extra gain on top of the limited number of RF chains by providing better options of inexpensive antennas in space.

Antenna selection. From theory to practice, equipping more antennas than RF chains, namely, antenna diversity, has attracted attentions due to the reductions in the hardware expenses [15], [31], [32], [33], [34]. Diverse algorithms have been proposed regarding various aspects including higher rank channel matrix [17], [35], [36], lower processing complexity [18], [19], compressed channel feedback[37], [38], and etc. Most recently we also see industry practices in this direction, e.g., Huawei smart antenna technology [22] enables switching between omnidirectional and directional antennas - however limited to only two antennas due to difficulty in channel sensing at run time. To the best of our knowledge, most existing algorithms are not experimentally studied in practice. Many studies have to assume practically in-affordable methods to gain perfect channel knowledge. How the augmented antennas can be supported by off-the-shelf Wi-Fi chipsets, including antenna scalability, adaptability to channel variation, and protocol compatibility, is not answered in previous studies, which is the core of WINAS.

Latest systems in Wi-Fi antenna augmentation. In [39], the authors propose a moving Wi-Fi AP, which moves across different locations to exploit spatial diversity gain. MIDAS [40] enables a distributed antenna system to benefit multi-user MIMO (MU-MIMO) in 802.11ac. How to augment commodity Wi-Fi and improve the built-in throughput of 802.11 is not addressed in the above two works. In [41], the authors presents a programmable radio environment, by instrumenting the environment with a large array of

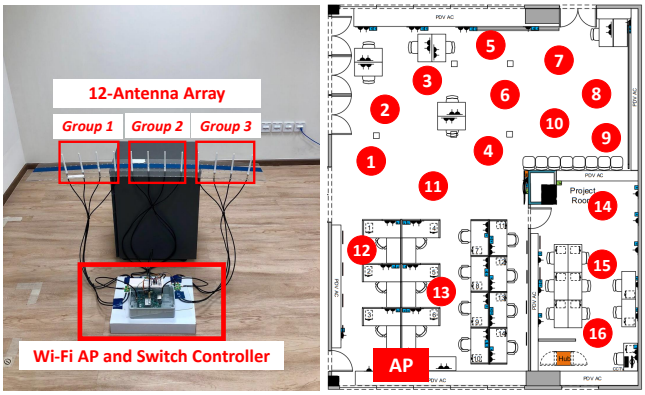

(a) Platform (b) Environment

Fig. 1. The platform and experiment environment.

antennas to manipulate the wireless channel. Multiple external antennas are introduced but attached to the environment, which is fundamentally different from the purpose of WINAS in improving transceiver side spatial diversity on commodity Wi-Fi terminals. An open-loop antenna selection scheme for Wi-Fi AP has been studied in [23], which is based on a special Wi-Fi model with only one redundant antenna for each of the three RF chains. A try-and-error solution is applied, which takes time at the order of seconds for probing and switching (WINAS in comparison achieves millisecond level switch). WINAS is a closed-loop system that enables fast antenna adaptation on commodity Wi-Fi APs and with the scale of the antenna array at a different level. In [42], the authors integrate multiple APs to serve multiple clients concurrently with a sophisticated synchronization design. When compared to [42], WINAS provides a solution in improving the overall capacity with a single AP, which is orthogonal in its design purpose and can be integrated the idea of [42] to further increase the capacity. Overall, WINAS is the first general antenna augmentation solution to commercial Wi-Fi AP and with compliance to standard PHY and MAC.

3 Motivation

We conduct preliminary measurement studies to investigate the potential gain from antenna augmentation. The gain is quantified by measuring downlink throughput of a Wi-Fi AP equipped with 12 augmented antennas. In the following, we show two types of measurement studies with two different points of view. 1) To show the potential of antenna augmentation, we study how the throughputs of different *AntComb*s for MIMO are diversified at various locations in a typical indoor environment. 2) Beamforming is another well-known approach to improve SNR by exploiting spatial diversity. To study how the beamforming gain overlaps with the gain of antenna augmentation, we compare their gain empirically with extensive measurements.

3.1 Experiment Setup

Platform. We conduct the measurement studies on both 2.4 GHz and 5 GHz Wi-Fi bands. For 2.4 GHz experiments, we let a commodity 802.11n NIC (WLE350NX) connect with an external antenna array and serve the Wi-Fi AP. The AP's three radio chains are connected with 12 COTS dipole antennas (each of cost less than $1), i.e., each radio chain has four candidate antennas, thus resulting in 64 different *AntComb*s in the case of 3x3 MIMO. For 5 GHz experiments, we use another commodity 802.11ac NIC (WLE1216V5) as Wi-Fi AP, which also supports beamforming. In both cases, for Wi-Fi client, we use the same NIC as that of AP, in its normal condition. Fig. 1(a) depicts the setup of the platform.

Environment. We conduct the experiments in our lab which represents a typical indoor environment as shown in Fig. 1(b). The Wi-Fi AP is deployed at the location highlighted in rectangle, and we selected 16 locations denoted in circled numbers, for deploying the Wi-Fi client. The locations of the clients are carefully selected to produce wireless channels covering three typical scenarios of indoor environment – LOS dominating, LOS existing and LOS blocked. By varying the location of the client, we evaluate the efficacy of antenna augmentation with the above different indoor scenarios. The experiments are conducted at night, thus with a relatively controlled environment.

Methodology. For each location of the Wi-Fi client, we measure downlink Wi-Fi throughput, for all the 64 *AntComb*s of 3x3 MIMO one by one, on both 2.4 GHz and 5 GHz bands. We use iPerf to measure the downlink throughput by generating a saturated UDP traffic at a relatively clean Wi-Fi channel. Each throughput result comes from a 60s measurement.

To quantify the spatial diversity gain, we define a metric

$$tpGain = \frac{max_{\forall i}\ throughput}{median_{\forall i}\ throughput} - 1,\ i = 1, 2, ..., 64 \quad (1)$$

where $tpGain$ and i indicate throughput gain and the index of *AntComb*, respectively. That is, $tpGain$ indicates the extra portion of maximum throughput compared with the median across 64 *AntComb*s at a given location, implying the throughput gain to exploit compared with the legacy fixed antenna case. The median throughput is used to represent the performance of the legacy fixed antenna systems because the different antenna combinations may lead to highly varied throughput which does not represent the overall performance. According to our measurement, the distribution of the median throughput measured with different clients' locations locates at the middle of the distribution of the throughput provided by different fixed antenna combinations, and therefore, the median throughput is representative.

3.2 Potential Gain of Antenna Augmentation

We show the throughput results across different *AntComb*s without beamforming. Fig. 2(a) shows the offered throughputs of different *AntComb* on 2.4 GHz and 5 GHz, respectively. The location that gives the highest $tpGain$ is ⑩ for both 2.4 GHz and 5 GHz. Specifically, the $tpGain$ values at the two frequencies are 0.90 (maximum: *AntComb* 64, median: *AntComb* 25), and 0.65 (maximum: *AntComb* 26, median: *AntComb* 9), respectively, meaning that 90% and 65% throughput improvement could be achieved in these cases by augmenting the antennas. Fig. 2(b) plots the $tpGain$ distribution across all the 16 locations on 2.4 GHz and 5 GHz bands, respectively. As the figure suggests, the $tpGain$

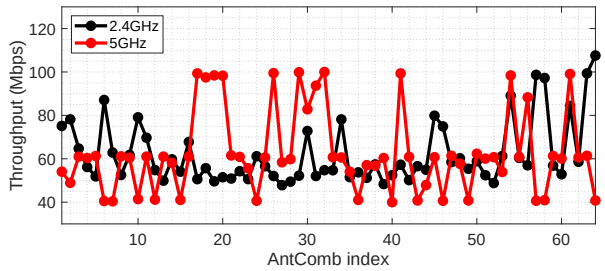

(a) Throughput results on 2.4 GHz and 5 GHz bands at location 10 which gives the highest $tpGain$

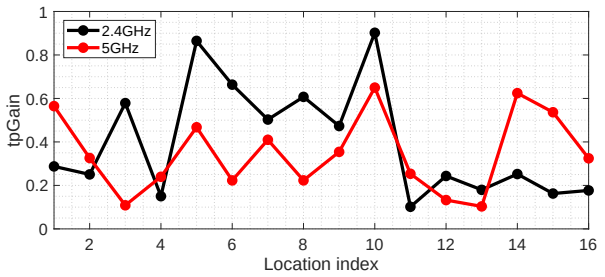

(b) $tpGain$s at various locations on 2.4 GHz and 5 GHz bands

Fig. 2. Throughput and $tpGain$ statistics on 2.4 GHz and 5 GHz bands.

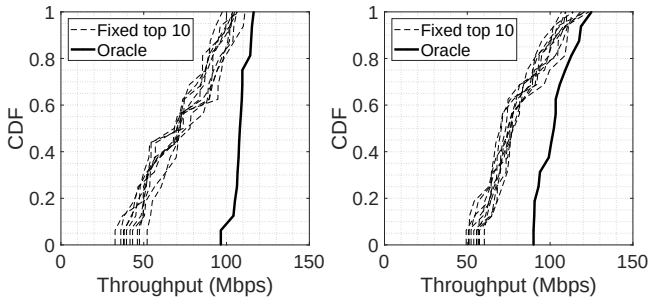

(a) 2.4 GHz (b) 5 GHz

Fig. 3. The potential of throughput improvement.

varies across different locations due to the different diversity of the multipath signals, and the average $tpGain$s are 0.40 (2.4 GHz) and 0.35 (5 GHz), across the 16 locations.

Fig. 3 summarizes the throughput distribution across the 16 locations in the case of adapting to the best *AntComb* at each location (Oracle), in comparison with those of top 10 fixed *AntComb*s. Fig. 3(a) and Fig. 3(b) show the empirical cumulative distribution function (CDF) of the results on 2.4 GHz and 5 GHz, respectively. In both cases, we see that the CDF curves of Oracle are confined within a narrow range, i.e., 97–116 Mbps on 2.4 GHz and 90–125 Mbps on 5 GHz, while with a fixed *AntComb*, even the best one, the CDF curves show relatively flat shapes, indicating the fluctuation of the throughput across different locations in both cases. On average there is a gap of 30 Mbps between the Oracle throughput and those of the top 10 *AntComb*s. This implies the significance of an intelligent *AntComb* selection and adaptation, which is the target of WINAS.

Impact of varied AP-client locations. The above results are obtained when deploying the AP at the corner of the room as shown in Fig. 1(b). To validate the throughput gain with different AP-client locations, we re-deploy the AP at the center of the room (near location ⑥), and repeat the throughput measurement with different client locations. We observe similar gaps of throughput improvement by as much as 40Mbps. As a matter of fact, due to channel

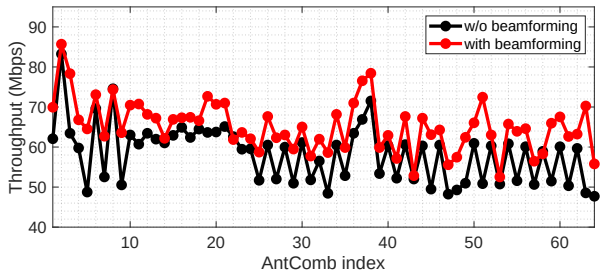

(a) The location with highest beamforming gain

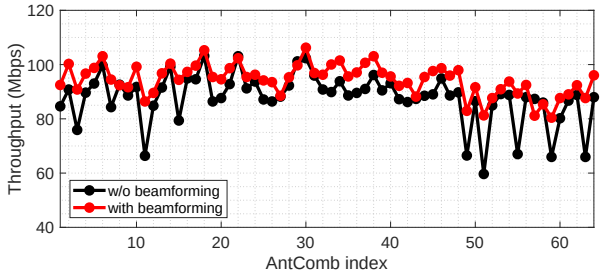

(b) The location with lowest beamforming gain

Fig. 4. Throughput results across different *AntComb*s with and without beamforming.

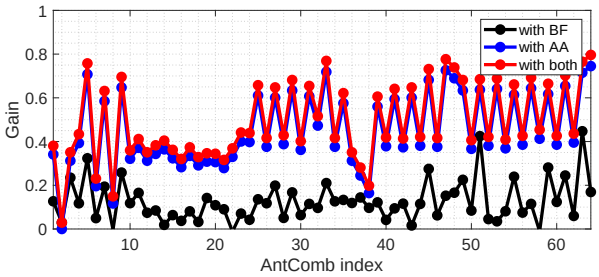

Fig. 5. Throughput gain of antenna augmentation, beamforming, and both

reciprocity varying the locations of the AP leads to equivalent antenna diversity gains as varying the locations of the clients.

3.3 Antenna Augmentation with Beamforming

We conduct further investigation to study whether the throughput gain brought by antenna augmentation overlaps with that exploited by beamforming. To this end, we measure the throughput with and without beamforming, with different *AntComb*s and at different locations.

Figs. 4(a) and 4(b) show the throughput results measured at locations ① and ⑨, corresponding to the locations yielding the highest and the lowest beamforming gain (throughput gap with/without beamforming enabled), respectively. In both results, the red and black lines represent the achieved throughputs from all 64 *AntComb*s with and without beamforming, respectively. We observe that, even with beamforming, the throughputs from all 64 *AntComb*s are highly diverse, demonstrating that the adoption of beamforming itself cannot fully absorb the gain introduced by antenna augmentation.

In a detailed study, Fig. 5 gives a comparison in terms of the potential gains brought by beamforming, antenna augmentation, and employing both schemes simultaneously, based on the throughput trace that we collect from location ①. The black line indicates the gain of beamforming, which is defined to the ratio of the throughput gap between

those with and without beamforming. The blue line indicates the potential gain of antenna augmentation, defined by the portion of the throughput gap compared between the best *AntComb* and each present *AntComb*. The red line indicates the improvement introduced by employing both antenna augmentation and beamforming. We see that the gain brought by antenna augmentation is substantial compared with that of beamforming, and more importantly, it is very close to that of employing both schemes simultaneously. This implies that the potential gain of antenna augmentation does not overlap with that brought from beamforming, specifically, it can provide further improvement atop beamforming by a factor of 1.2x in 802.11ac.

The rationale of the gain. Wi-Fi derives the beamforming weights with Singular Value Decomposition (SVD), which separates the concurrent spatial streams that are entangled with wireless channel, and maximizes the effective SNR for the derived parallel, independent sub-channels [43]. The upper bound of the maximization is decided by the spatial correlation between the signals received at the multiple radio chains. The design of antenna augmentation further gains on top of beamforming because it provides more potential channels with lower correlation, and therefore produces higher effective SNR for the beamformed channel.

3.4 Summary

Our empirical study shows the potential gain of antenna augmentation by considering two aspects: 1) When compared with legacy fixed antenna MIMO, up to 1.90x and 1.65x higher throughput can be offered on 2.4 GHz and 5 GHz, respectively. 2) The gain of antenna augmentation does not fully overlap with that of beamforming, and hence, adds to beamforming by a factor of 1.2x. These results cement the rationale of designing WINAS for Wi-Fi antenna augmentation.

4 System Design

4.1 Overview

WINAS is implemented at AP, which is supposed to serve normal Wi-Fi clients. That is, WINAS targets at improving the downlink[1] Wi-Fi throughput, by controlling *AntComb* at AP side in real-time. Clients being served can be WINAS-agnostic normal Wi-Fi devices, e.g., smartphone, without any modification to their hardware or software.

The hardware architecture adopted by this work consists of a commodity Wi-Fi AP augmented by an external 12-antenna array as illustrated in Fig. 6. To ensure that the Wi-Fi AP can select *AntComb* on demand in a fast and reliable way, we build our hardware architecture primarily on top of SWAN [32], with extra hardware efforts for further improved hardware efficiency and reliability (see Section 4.2).

WINAS serves the associated client with an *AntComb* that is most likely to achieve the highest downlink throughput among all possible *AntComb*s. WINAS operates alternately in two working states, namely, *searching* and *serving*. In *searching* state, an efficient sounding operation is conducted to promptly identify the best *AntComb* (finished in milliseconds), while in *serving* state, normal Wi-Fi service is provided with the identified *AntComb*.

1. The design of WINAS focuses on downlink traffic which takes over 80% of the total Wi-Fi traffic [44].

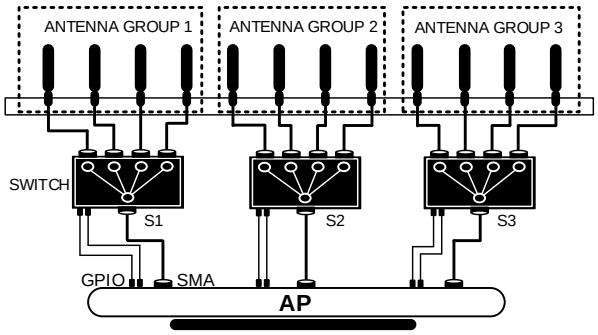

Fig. 6. WINAS hardware architecture.

The design of WINAS addresses the following three technical challenges. 1) It is essential to promptly estimate the expected throughputs of all possible *AntComb*s so the *searching* state can be minimized. WINAS employs a CSI-based throughput estimation scheme to promptly identify the best *AntComb* and switch to it (Section 4.3). 2) *AntComb* needs accurate timing in alternating between searching and serving to achieve the best efficiency, and that requires adapting to the trend of channel variation. A machine learning model is developed to derive the right moment for triggering searching state (Section 4.4). 3) Change of *AntComb* may be followed by an abrupt improvement of channel quality, but the legacy PHY-rate control algorithm, e.g., Minstrel [45], [46], lacks fast adaptation to that. WINAS incorporates a light-weight modification to Minstrel that enables fast PHY-rate follow-up (Section 4.5).

4.2 Prerequisite

Hardware architecture. As Fig. 6 illustrates, in current prototype, a single-pole-four-throw RF switch (Peregrine PE42442) is used to connect each radio chain of the AP to four external antennas through coaxial cable (RG 50). We use three RF switches to form a 12-antenna array. As such, at each moment, each RF switch can relay the signal between one of the four candidate antennas and a radio chain. The AP controls the output ports of the three RF switches directly, through the GPIO pins on its board by sending a two-bit command to each of them. The control delay is much shorter than that of SWAN, where the AP controls RF switches indirectly via an Arduino [32]. In order to further reduce the control delay, we embed the control command into the Linux kernel. By that, we reduce the switching delay from 29μs of SWAN [32] to below 4.5μs.

Prerequisites for AP. To adopt WINAS, there are following prerequisites. 1) The AP needs to support CSI manipulation. This is available to industrial manufacturers who possess full access to the PHY of Wi-Fi, and has been recently made available to research community on many commodity AP models thanks to previous work on CSI extraction on 802.11n [47] or 802.11ac [48]. 2) AP's user and kernel space functions are programmable. Most commodity APs operate with open source linux distributions (e.g. OpenWRT, asusWRT), and meet such a requirement. 3) The AP's board should support output signaling through interfaces like GPIO (adopted in this work), Ethernet [32],

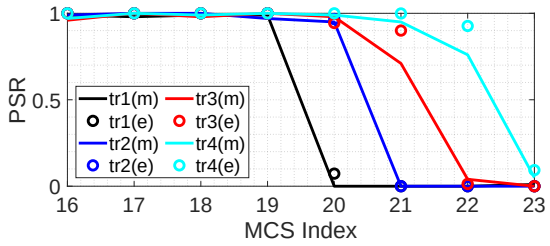

Fig. 7. PSR comparison between estimated and measured.

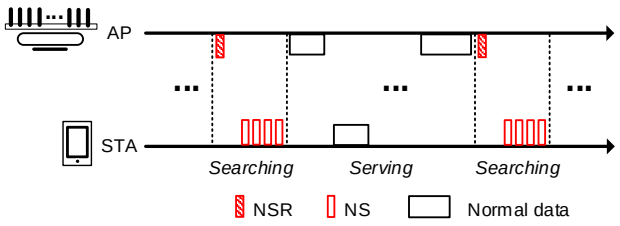

Fig. 8. Searching and serving states in WINAS.

or USB, and equip detachable antennas, which is prevalent for commodity APs. Many off-the-shelf APs fulfil the above requirements, e.g., TP-Link WDR4310, Compex WPJ563, Asus RT-ac86u, etc. [49].

To facilitate the delivery of our core idea, in the following, we take a single Wi-Fi client case to elaborate WINAS. In our current prototype, 802.11n/ac AP is used due to the readily available CSI extraction function for 802.11n/ac [47]. We provide detailed discussion on multi-user support and the potential integration with latest 802.11ax standard in Section 6.

4.3 *AntComb* Selection

In identifying the best *AntComb* that yields the highest Wi-Fi throughput, it is essential to promptly estimate the expected throughput of each *AntComb*, whereby the best one can be selected. Intuitively, it may be achieved by probing with adequate Wi-Fi packets, and analyzing the packet delivery statistics. Such an approach, however, incurs substantial probing overhead and, consequently, results in considerable probing delay ([23] uses probing period of 5 sec), which is unacceptable in WINAS since *AntComb* selection must be completed in minimized searching state and otherwise impair normal data traffic.

For that reason, WINAS takes a different approach. WINAS uses CSI and applies a model driven approach to quickly estimate the throughput. For a given *AntComb*, all necessary CSI can be obtained with a single probing packet, thus avoiding cumbersome lengthy data collection.

CSI-based throughput estimation. CSI, in essential, tells the quality of the incoming signal resulted from the wireless channel, which in turn can link us to the expected throughput. Mathematically, throughput can be expressed as

$$TP = \frac{PL \times PSR}{E[DUR]}, \tag{2}$$

where PSR and DUR denote packet success rate and the time interval between the preamble of two consecutive packets, respectively. PL denotes packet length, which is decided before transmission. PSR is equal to $(1-BER)^{PL}$, where BER represents the bit error rate of the packet. DUR and BER are illustrated as follows.

$$DUR = \text{DIFS} + \text{E[BO]} + Dur(\text{DATA}) + \text{SIFS} + Dur(\text{ACK}), \tag{3}$$

Eq. 3 is defined based on the operation of CSMA/CA [50]. In Eq. 3, DIFS/SIFS and Dur(ACK) use fixed values of frame spacing and ACK duration, which are defined with CSMA/CA protocol. Dur(DATA) denotes the duration of data frame and is known to the transmitter. E[BO] represents the expected transmission back off time, which is determined by the MAC channel contention, and is obtained by averaging the number of back offs measured during a previous time window.

Based on the relationship between BER and SNR in AWGN channel [51], we have

$$BER = \alpha \times Q(\beta \times eSNR), \tag{4}$$

where α and β depend on the modulation scheme [52]. We use the concept of $eSNR$ (effective SNR) [53] in Eq. 4, a more comprehensive metric than SNR that takes the impact of spatial correlation and frequency selective fading into consideration in assessing MIMO-OFDM link quality. To compute $eSNR$, in addition to follow the method proposed in [54] that simulates the effect of MIMO processing gain (MMSE for multiplexing and MRC for diversity [51]), we also consider the impact of FEC coding on standardized coding rate by applying NIST error rate model [55], [52].

Previous illustration is based on using a specific PHY-rate. In practice, Wi-Fi defines different PHY-rates denoted by different modulation and coding scheme (MCS) indices,[2] to adapt to different signal qualities. Different PHY-rate results in different throughput estimation due to different PSR (caused by different BER) and DUR (caused by different $Dur(DATA)$) in Eq. 2. The final expected throughput can thus be selected from all TP estimations based on the 24 different MCS choices:

$$TP_f = \max_i(TP_i), i = 0, 1, 2, ..., 23 \tag{5}$$

where TP_i indicates the estimated throughput with MCS i.

We perform trace driven analysis to compare the estimated PSR and the measured PSR. Fig. 7 depicts the results from four different traces (of different $eSNR$s) that cover MCS index 16–23. The results suggest high accuracy of PSR estimation (denoted as 'e') from a single packet in comparison with measured empirical statistics (denoted as 'm') based on 1000 probing packets.

Searching and serving. WINAS entails a *searching* state, which is triggered intermittently on demand during Wi-Fi *serving* state. Specifically, in *searching* state, a Wi-Fi client sends N short probing packets, namely, null data sounding (NS) packets, sequentially, triggered by an NS Request (NSR) packet sent by Wi-Fi AP. The Wi-Fi AP iterates over the N different antennas connected to each of its radio chains, to receive each of the probing packets, where N is set as the total number of candidate antennas of each radio chain, i.e., 4 in current prototype. As a result, after receiving N NS packets, the CSI regarding all the external antennas has been collected for throughput estimation. In

2. In 802.11n, there are 24 different MCS choices and the MCS index ranges from 0 to 23 [1].

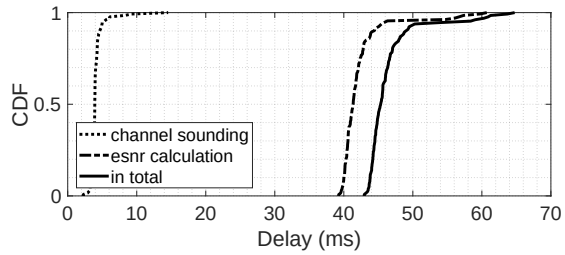

Fig. 9. Delay measurement in searching operations.

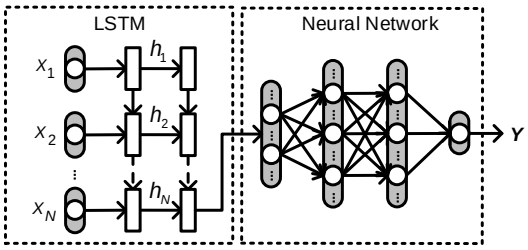

Fig. 10. LSTM based neural network for predicting the throughput gains.

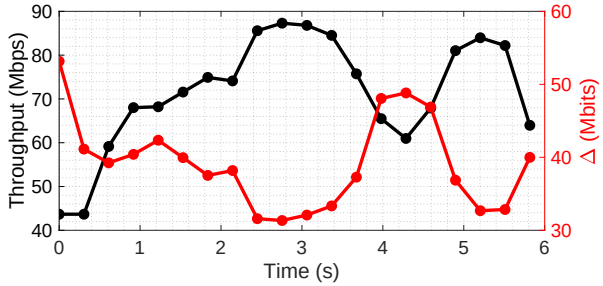

Fig. 11. Predicted throughput gain v.s. measured present throughput.

serving state, Wi-Fi AP provides normal Wi-Fi service with the *AntComb* selected as the best one by the throughput estimation model. Fig. 8 illustrates the above operations. The NSR and NR packets can be embedded into some existing protocol flows, e.g., Wi-Fi beamforming (see Section 6), TCP synchronization, or QUIC control messages [56]. We experimentally study the time delay imposed by above operations in *searching* state and plot the results in Fig. 9. As the results suggest, the channel sounding operations take an average of 4ms in total which defines the *searching* state and brings minimum impairment to normal data traffic. The $eSNR$ computation and throughput estimation takes an average of 41ms, which is the lag before WINAS switches to the best *AntComb*. Nevertheless, in the meantime of throughput estimation (4ms–41ms) WINAS has already entered serving state and started data traffic (with the previous non-optimal *AntComb*). The searching operation (as well as the timing design we will introduce in Section 4.4) runs in parallel to Linux networking stack, so any searching delay does not harm to normal packet flows but only delays the gain of serving with the best *AntComb*, which our experiment results verify in Section 5.2. In summary, at the end of the *searching* state, the expected throughputs of all *AntComb*s are derived, among which the *AntComb* with the highest throughput is selected to serve the data traffic until the next *searching* state. Detailed experimental study of the throughput estimation and *AntComb* selection performance is provided in Section 5.1.

4.4 Timing the searching

In WINAS operation flow, if *searching* state is triggered excessively, sounding overhead will impair the throughput gain delivered by the better *AntComb*, while if *searching* state is not triggered in time, the AP will miss opportunities in adapting the selected *AntComb* to the channel variation, which essentially limits the diversity gain we can exploit.

In addressing the above challenge, we need to first establish a criteria to assess the benefit of triggering a *searching* state. To this end, we compare *loss*—the throughput loss caused by sounding overhead during *searching* state—and *gain*—the throughput gain ascribed to adopt a better *AntComb* after triggering a searching state. The loss calculates as

$$loss = \int_{t_0}^{t_1} TP_c(\tau)d\tau \tag{6}$$

where t_0, t_1 denote the start and end of the *searching* state, respectively, and $TP_c(\tau)$ denotes the expected throughput of current *AntComb* at time τ, indicating the amount of traffic loss due to *AntComb* search between t_0 and t_1. The gain calculates as

$$gain = \int_{t_1}^{t_2} TP_b(\tau) - TP_c(\tau)d\tau \tag{7}$$

where t_2 indicates the end of the coherence time starting from t_0, and $TP_b(\tau)$ indicates the expected throughput of the best *AntComb* at time τ. Apparently, if the gain outweighs the loss, triggering a *searching* state at t_0 is beneficial. We add a conservative margin γ (empirically set to 45 Mbits) to avoid ping-pong effect, i.e., the condition for triggering searching state is $\Delta > \gamma$, where Δ equals $gain - loss$, and quantifies the throughput improvement due to the selected antenna combination from time t_1 to t_2, in compensation to the overhead of channel sounding from time t_0 to t_1.

To employ the above strategy, WINAS needs to predict Δ in real time. A Long Short-Term Memory (LSTM) based neural network model is applied to make the prediction. LSTM has been widely adopted for time series prediction due to its capability of memorizing past information, and based on which to make future prediction. In the case of Wi-Fi throughput gain prediction, since it varies continuously due to the temporal correlation of wireless channel [57], [58], LSTM is a proper choice in incorporating the correlated throughput gain variation.

Fig. 10 gives the detailed structure of the neural network. The model contains two LSTM layers and three fully connected layers. The output length of the first LSTM layer is 32, the output length of the second LSTM layer is 16, and the last softmax layer contains one normal neural node.

WINAS keeps deriving the $eSNR$s of every data packet during serving state, and feed the $eSNR$ samples from the most recently received 20 packets to the model as the input vector. The output is Δ. In serving state, on receiving every new data packet, WINAS derives a new Δ and compare with γ to make a decision on whether triggering the *searching* state or not.

To train the model, we collect $eSNR$ samples from packets received by Wi-Fi AP with a 30-minute real world measurement conducted under a controlled environment

occupying an area of about $200m^2$. During the measurements, we move a client along a random path at a speed of about 1 m/s which continuously transmits about 1000 packet/s to the AP. The preprocessing of the collected dataset includes 1) re-sampling the $eSNR$ with a sampling rate of one kHz to make it evenly distributed in time, and 2) segmenting the output of the re-sampling with a moving window of size 20, which constructs ∼1.8 million samples with the smallest moving stride. The label of each training sample is provided by applying Eq. 6 and Eq. 7, where the $TP_b(\tau)$ curve is derived from measurement results of intermittently conducted *searching* states using interpolation, as TP_b does not vary much over time. We perform a trace driven analysis to show the effectiveness of the model in predicting Δ. Fig. 11 presents the predicted Δ (in red) along with the time and compares it with the measured throughput TP_c (in black) of one *AntComb*. we can see clear trend of Δ oppositely related to the trend of TP_c in time, implying timely suggestion from our model for triggering the *searching* state.

The machine learning model adopted in WINAS is light weight. The implementation of the machine learning model contains two LSTM layers and three fully connected layers. The total number of parameters contained in the model is 8645, and the total size of the model is only 121 kB. During run time, the memory consumption of the model inference is 33 kB, which consumes only 0.03% of the system memory of our prototyped device (Atheros WPJ558 with 128 MB DDR2).

The model does not need to be re-trained as long as the physical channel varies in a continuous way. The reason is that, the LSTM model is designed to learn the trending of variations, specifically the physical wireless channel variation in WINAS. The model is thus able to capture the continuity of the variation, based on which it infers the futural channel condition with time-series prediction. Note that the continuity of the wireless channel variation has been validated by many existing works [58], [59], and is not affected by sporadic update of the environment (e.g., new furniture installed in the environment).

4.5 Rate Adaptation

While WINAS is able to identify and switch to the *AntComb* that provides the best channel, the actual throughput improvement relies on a quick adaptation of the PHY-rate to exploit the improved channel quality. WINAS can work seamlessly with legacy 802.11n PHY-rate control algorithm, which is able to adapt the PHY-rate to the current channel quality based on historical packet statistics.

Default 802.11 rate control algorithm, e.g., Minstrel, however, lacks fast adaptation due to its statistics based nature, which is unfavorable in exploiting the sudden channel improvement brought by the change of *AntComb*. WINAS optimizes the interactiveness between *AntComb* and PHY-rate adaptation to further improve throughput.

The core idea is to confine the range of the candidate PHY-rates and put more weights on more likely candidates based on the knowledge that WINAS has learnt about the channel, thus reducing the convergence time. Instead of enforcing an optimal rate based on instantaneous CSI readings, our choice of conforming with Minstrel allows compatibility and inherits its resilience with channel jitters.

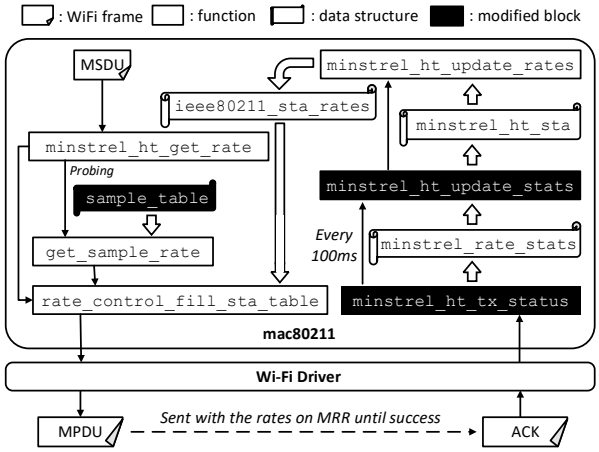

Fig. 12. WINAS modification to the conventional Minstrel rate adaptation algorithm.

Specifically, conventional Minstrel infers the optimal PHY-rate, based on historical PSR statistics. During each 100ms interval, Minstrel probes all the MCS indices within a randomly initialized MCS table and at the end of each interval, the PSR of each MCS is updated with a weighted moving average, i.e.,

$$p_R(t+\Delta t) = (1-w)p_R(t) + w\frac{S_R}{T_R} \tag{8}$$

where $p_R(t+\Delta t)$ denotes the PSR of PHY-rate R at time $t+\Delta t$, and S_R, T_R denote the numbers of successfully received and transmitted packets (probing and/or normal data) with PHY-rate R during the most recent 100 ms, respectively. A typical value of the weight w is 0.96.

To confine the candidate PHY-rates, at the end of each *searching* state, WINAS modifies the MCS table used for probing to only contain indices greater than the previous optimal PHY-rate, which is based on the fact that the optimal PHY-rate after an *AntComb* selection will always be greater than the previous one, thus removing unnecessary probing and its negative effect on PHY-rate convergence. Also, the previous PSR value, i.e., $p_R(t)$ in Eq. 8, is set to 0 for the MCS indices within the range of probing. By doing so, the impact of the historical statistics associated with the previous *AntComb* is removed, thus achieving a more aggressive PHY-rate adaptation to the newly selected *AntComb*. The implementation of WINAS modifications are embedded into the 802.11 driver in Linux kernel that contains Minstrel as shown in Fig. 12 (with the relevant functions and structures highlighted in black).

5 Evaluation

We evaluate WINAS by firstly demonstrating the effectiveness of the three building blocks, i.e., accuracy of *AntComb* selection, efficiency in triggering the *searching* state, and rate adaptation, followed by end-to-end system evaluation with various different real world scenarios.

5.1 *AntComb* Selection

The accuracy of *AntComb* selection relies on the accuracy of throughput estimation. In the following, we start with the evaluation on throughput estimation of WINAS.

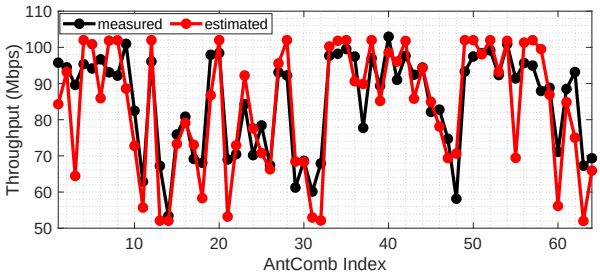

Fig. 13. Est. throughput compared with the measured ground truth.

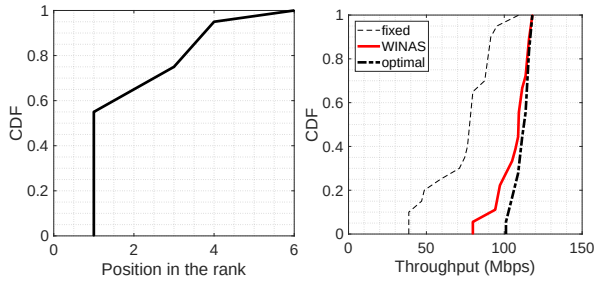

(a) Ground truth ranking of the selected *AntComb*

(b) Throughput comparison

Fig. 14. Accuracy of *AntComb* selection.

The experiment takes place in the lab space with the environment as shown in Fig. 1(b), where a WINAS-enabled Wi-Fi AP is deployed at the location highlighted in rectangle, and we select 16 locations denoted in circled numbers to deploy the Wi-Fi client. For each location, we measure the downlink throughput with each of the 64 *AntComb*s for 60s.

Throughput estimation. Fig. 13 plots an experiment trace showing the accuracy of throughput estimation, by comparing the estimated results with the measured on corresponding *AntComb*s. The estimation correctly predicts the peak (e.g., *AntComb*s with index 20, 36, 54) and valley (e.g., *AntComb*s with index 11, 31). For most of the cases, the estimation errors are under 10 Mbps, and they never lead to fatal mistakes on choosing a "good" *AntComb*, because rather than the precise value of any single estimation, it is the relative value of throughput estimations over *AntComb*s that decides the correctness of antenna selection.

***AntComb* selection.** We evaluate the accuracy of *AntComb* selection, by identifying the ground truth ranking of the selected *AntComb* by WINAS. For comprehensive assessment, we summarize the results measured from all 16 locations. Fig. 14(a) shows the CDF of the ground truth ranking of the selected *AntComb*. For over 50% of the measurements, the selected *AntComb* provides the best performance, it stays in top three for near 80% of the cases, and within top six for all measurements, which suggests high accuracy of *AntComb* selection considering the selection is conducted among 64 *AntComb*s. Fig. 14(b) shows the CDF of the throughput produced by selected *AntComb*s at the 16 locations (solid line), and compares that with the optimal case, i.e., the set of the highest measured throughput of corresponding locations (thick dotted line), and that of the best fixed[3] *AntComb* (thin dotted line). On one hand, the CDF curve of WINAS selected *AntComb* is very close to that of the optimal, with a gap of below 20 Mbps in the worst case.

3. Best fixed *AntComb* is a fixed set of antennas that offers the highest averaged throughput over all locations.

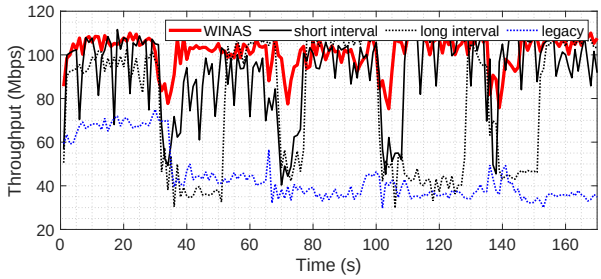

Fig. 15. Throughput measurement for different timing schemes.

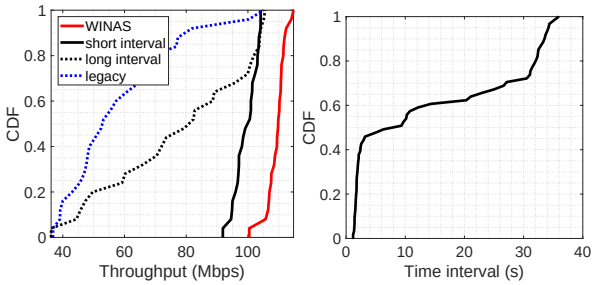

(a) CDF of the averaged throughput across locations.

(b) CDF of the interval between consecutive *searching* state in WINAS.

Fig. 16. 30 minute measurement study within a $200\ m^2$ area.

On the other hand, the CDF curve of WINAS outperforms that of the fixed *AntComb* by over 40 Mbps in the worst case.

5.2 Efficiency of Timed Searching

WINAS predicts the throughput gain and based on that triggers the *searching* state. We show the efficiency of WINAS's timed searching by comparing that with a baseline scheme, i.e., the AP enters *searching* state periodically.

During the experiment, we walked the client randomly in a move-and-sojourn method, to mimic practical Wi-Fi usage patterns. A number of locations within the lab space were selected where the client sojourns during the walk. The transitions between the locations were randomly decided, and the duration of the sojourn at each location followed a Gaussian distribution with the average of 30s. This experiment is repeated three times - one with WINAS and the other two with baseline schemes having different *searching* intervals, i.e., 5s and 25s, representing different level of channel variation.

Fig. 15 depicts a three-minute trace of measured throughputs of the three schemes. For comparison, we also put the throughput trace measured with legacy scheme on a fixed *AntComb*. As expected the throughput of WINAS shows the skyline, which remains at over 100 Mbps for ∼85% of the time. To show a more comprehensive comparison, we extend the same methodology to a larger space occupying the entire area of about $200m^2$ in the lab space and conduct the experiment for a duration of 30 minutes. Fig. 16(a) plots the CDF of the averaged throughputs of different schemes. Comparing with the periodic timing schemes using long (25s) and short (5s) intervals, the throughput gain of WINAS's adaptive timing scheme is 1.38x and 1.12x, respectively. When compared with the legacy scheme using fixed antennas, WINAS achieves 2.09x throughput gain. Specifically, the throughput provided by WINAS stays at high level, i.e., within 100 Mbps to

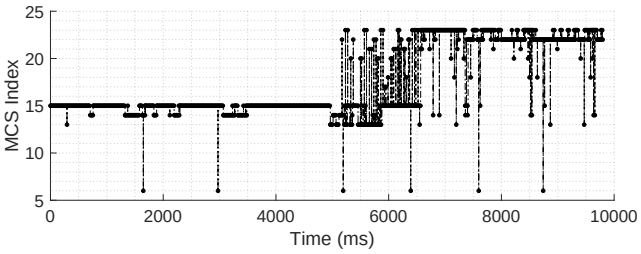

(a) Rate adaptation with conventional Minstrel

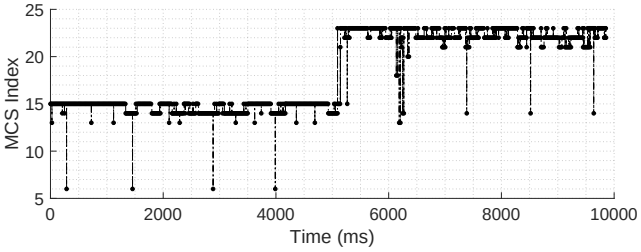

(b) Rate adaptation with WINAS modified Minstrel

Fig. 17. Example trace of rate adaptation after antenna selection.

115 Mbps. To provide more details, Fig. 16(b) shows the CDF of the time intervals between consecutive *searching* states in WINAS. The figure shows that the time intervals are mainly distributed in two clusters around 2s and 30s, respectively, which is in line with our move-and-sojourn pattern with mean sojourn time of 30s, demonstrating the efficiency of WINAS in adapting to channel variations.

5.3 Rate Adaptation

In this section, we compare WINAS with conventional Minstrel adopted in Wi-Fi and identifies the effecacy of the fast PHY-rate follow-up after a *searching* state.

Figs. 17(a) and 17(b) depict snippets of MCS index traces with conventional Minstrel and WINAS modified Minstrel, respectively. In both traces, a *searching* state is triggered at the packet of index 5000. We can clearly see that the original Minstrel starts to probe packets with various PHY-rates and converges to the optimal PHY rate slow, while, with WINAS, the PHY-rate promptly converges to the optimal value. Fig. 18 presents the statistics on WINAS improvement on rate adaptation delay as well as on its delivered data volume. Fig. 18(a) shows the CDF of the reduced convergence time by WINAS. In more than 50% cases, the reduction is greater than one sec., demonstrating the effectiveness of WINAS on fast PHY-rate adaptation. The extra data volume delivery due to the fast convergence of WINAS is derived by integrating the PHY-rate difference during the convergence period. Fig. 18(b) shows the CDF of the extra data volume delivery, which shows, in more than 50%, 7 Mbits extra data can be additionally provided for each switch.

5.4 End-to-End System Evaluation

To evaluate the end-to-end system performance of WINAS in practice, we first experimentally examine three major factors: 1) mobility, 2) environment, 3) multi-client, and then conduct experiments based on the real usage patterns of different Wi-Fi users, to reflect the performance in real world.

Different mobility. To reflect different mobility, we introduce Motion Ratio (MR), defined as the ratio of movement

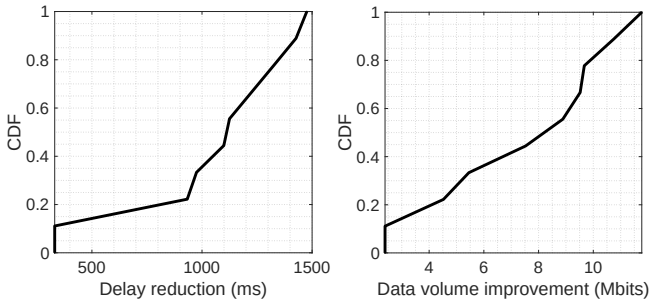

(a) Reduction on the rate adaptation delay (b) Extra delivered data volume during rate adaptation

Fig. 18. Improvement of WINAS modified Minstrel.

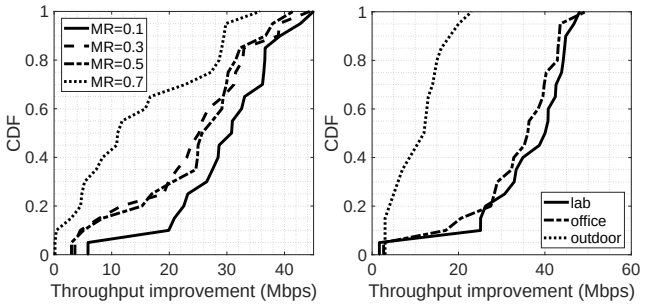

(a) Throughput improvement with different MR. (b) Throughput improvement with different environments.

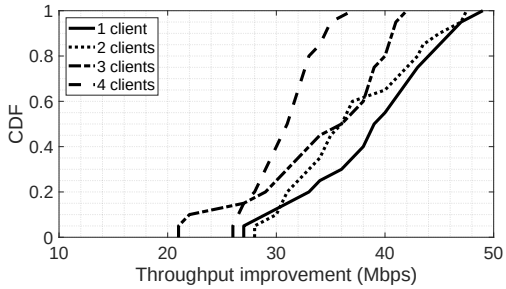

(c) Throughput improvement with multiple clients.

Fig. 19. Throughput improvement with different MR, environment, and number of mobile clients.

time over the entire Wi-Fi usage time. We measure the throughput improvement achieved by WINAS with four different levels of mobility, with MR increasing from 0.1 to 0.7 with the step of 0.2. Figure 19(a) shows the CDF of the improved throughput by WINAS over legacy Wi-Fi. When MR is 0.1, the throughput improvement is greater than 25 Mbps in 80% of the cases. With the increase of MR, the throughput gain decreases, due to the fact that the convergence speed of the rate adaptation cannot follows channel variation, especially, in indoor environment with MIMO. Even that, WINAS can still make improvement of greater than 10 Mbps with 60% test cases when MR equals to 0.7.

Different environment. We consider three different types of environment, i.e., a lab space with few environment dynamics (as shown in Fig. 1), crowded office (as shown in Fig. 20) during working hours, and an outdoor corridor. For each environment, we measure throughput at each of 15 selected locations with and without WINAS enabled. For the static lab space, the throughput is improved by more than 30 Mbps in 80% cases, as Fig. 19(b) indicates. The improvement with a crowded office is slightly lower

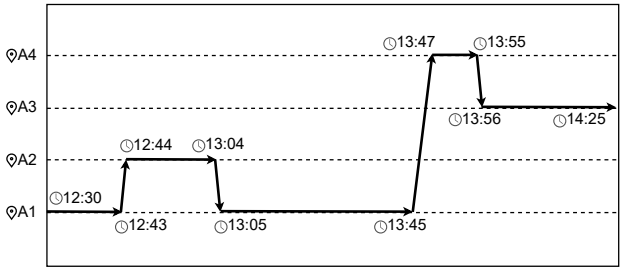

(a) Wi-Fi usage profile recorded by smartphone user 1.

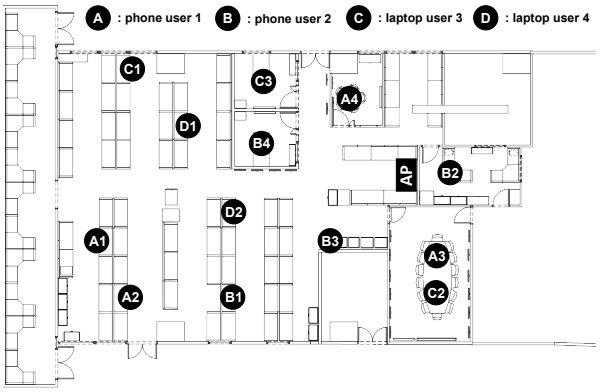

(b) The floor plan of the office environment, and the representative locations where the users are primarily active when using Wi-Fi.

Fig. 20. The methodology and environment of the real-world experiment.

but still with more than 25 Mbps improvement achieved in 80% cases. In the outdoor environment, the improvement is more than 5 Mbps in 80% cases, which is much lower when compared with the indoor experiment due to the reduced diversity in open space.

Multiple clients. We measure the throughput improvement for multi-client scenario where the number of associated clients increases from one to four. The improvement is quantified as the aggregation of throughput gains over all clients. Fig. 19(c) depicts the results. Overall, for over 80% of the measurements, the averaged improvement over the four cases is ∼30 Mbps. The throughput improvement gets narrower with the increasing number of clients mainly due to the higher overhead of packet switching control. It is still able to achieve 31 Mbps throughput improvement in median with four clients. Another observation is that the improvement becomes steadier with increased number of mobile clients, probably because when the mobile clients scatter in space, the overall diversity gain gets steadier.

Real-world Evaluation. To reflect the real-world performance of WINAS, we conduct experiments based on the real usage patterns of different Wi-Fi users. To do so, we firstly collected the traces of four volunteers when they use Wi-Fi for Internet in typical office environment. Two of them contributed their traces of smartphone usage profiles, and the other two contributed their laptop usage profiles. Fig. 20(a) provides an example of the trace recorded by smartphone user 1. As the figure depicts, the user used Wi-Fi from 12:30 to 12:43 at location A1, moved to location A2 from 12:43 to 12:44 (during which kept using Wi-Fi), and then used Wi-Fi from 12:44 to 13:04 at location A2. The user also moved to location A3 and A4 with continuous Wi-Fi usage. In fig. 20(b), we plot the floor plan of the test

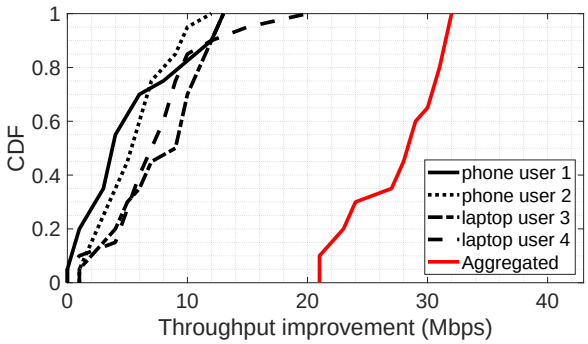

Fig. 21. Throughput improvement measured with real world use cases from four volunteers.

office. We indicate the locations where the prototype AP is deployed, and the representative locations where the users actively use Wi-Fi.

After obtaining the Wi-Fi usage profiles of the four users, we mobilize an Atheros Wi-Fi router (for extracting the CSI with the Atheros CSI tool) to repeat the recorded Wi-Fi usage trace for each of the four users. The MIMO configuration is fixed to be the same as used in each of the user devices to exactly emulate the Wi-Fi usage profiles. With all four users simultaneously associated with the prototype AP, we measure each individual's throughput gain, and plot the result in Fig. 21. We observe that firstly, the measurements of throughput improvement are all positive, which indicate that WINAS always provides better throughput than legacy scheme for all four Wi-Fi users at all time. Secondly, the improvements of the two smartphone users are slightly lower than those of laptop users because they normally use less antennas and experience higher mobility. The averaged throughput gain among all four users is 1.45x for half of the measurements. Even in the case with lowest improvement, i.e., for smartphone user 1, WINAS still provides 1.25x (from 16 Mbps to 20 Mbps) throughput improvement for 50% of the time. In the case of user 3, WINAS improves the throughput by 1.6x (from 15 Mbps to 24 Mbps) for 50% of the time. On average, the throughputs of the four users are improved by 1.37x, 1.43x, 1.53x, and 1.56x, respectively. We also plot the aggregated throughput improvement among the four users to show the overall performance. As illustrated with the red curve, WINAS 1.44x (from 64 Mbps to 92 Mbps) gain of the aggregated throughput in median.

6 Discussion

Supporting multiple clients. Concurrent support for multiple clients is desirable for practical Wi-Fi usage. The searching-serving design of WINAS can be easily extended to multi-client support. The AP may maintain a configuration profile for each client device. During runtime, the profile records the time varying CSI structure and keeps updating the best *AntComb* for the downlink channel of each client. With the client customized profile, the AP makes timing decision and conducts *AntComb* switching. A one-for-all *AntComb* is used for all uplink transmissions over different clients, and the *AntComb* is selected based on maximum average uplink throughput from all clients. Fig. 22 illustrates this design. The maintenance and update of each client profile runs in parallel thread to avoid latency.

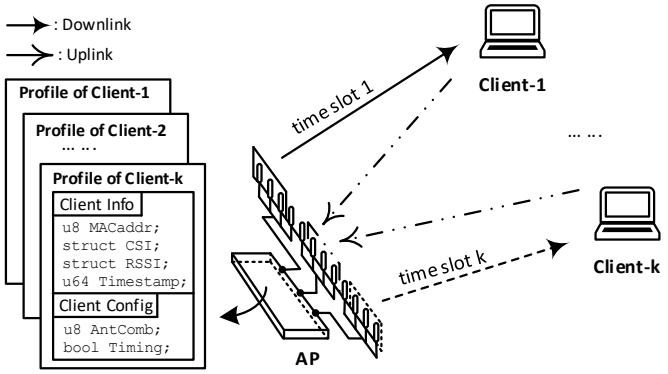

Fig. 22. WINAS multiple clients support.

In such design, the client specific uplink traffics that AP uses for channel sampling are mixed in time and across clients. We find that the scheme complies with Wi-Fi Air Time Fairness (ATF) [60], which is a standard scheme to maintain fairness among associated clients, and operates to serves each client during an allocated time slot. We adapt our scheme to ATF by embedding fast searching into the dedicated time slot of each client, in order to isolate the channel samplings from different clients. Note that all WINAS operations are based on general Wi-Fi frames and thus follow standard Wi-Fi medium access procedures. Communication with multiple clients does not compromise the execution flow of WINAS. We evaluate WINAS performance with multi-client scenario in Section 5.4.

Embedded into beamforming. We have tested WINAS performance with 802.11n and believe it can be applied to 802.11ac with access to the CSI. Beamforming is a mandatory operation required for all 802.11ac compatible APs, and WINAS can be perfectly embedded into beamforming operational flows. The Null Data Packet (NDP) sounding is the sole beamforming method offered in the standard, in which the AP as the beamformer sends NDP sounding packet and requests for explicit feedback matrix from beamformee every time before starting normal data traffic. WINAS *searching* state can be embedded into NDP sounding without introducing extra protocol overhead. As the NDP sounding is a MAC layer operation, embedding WINAS into beamforming makes it transparent to upper layers.

Potential integration with 802.11ax. As described in Section 4.2, the current implementation of WINAS is based on 802.11n hardware mainly due to the constraint on the accessibility to CSI extraction and kernel programming with 802.11ax devices. When integrated with 802.11ax, we believe that WINAS would still benefit the COTS devices, and could create additional design space for further improvement. Specifically, we expect that: 1) The throughput gain provided by antenna augmentation would remain or even increase for 802.11ax. The reason is, 802.11ax adopts the higher modulation rate of 1024 QAM. The denser constellation of the high modulation rate needs to be supported by higher SNR of the physical channel, which may greatly benefit from the spatial diversity gain from WINAS. 2) The proposed antenna augmentation can be organically combined with the main technical advances (e.g., OFDMA, spatial frequency reuse) of 802.11ax to provide better performance. For example, OFDMA segregates the spectrum into time-frequency resource units (RUs), which would be allocated by the network coordinator (i.e., the AP) to its associated stations to achieve concurrent packet transmission or reception. Antenna augmentation, when combined with such a technique, may enrich the content of resource unit by introducing another dimension of antenna space to the original time-frequency block, and thus leads to higher degree of freedom for resource allocation. In general, antenna augmentation complies with 802.11ax aspiration of resource reusing well.

To make the proposed system better adaptable to 802.11ax standard, some technical designs may be slightly adjusted. In order to implement the network functioning (e.g., uplink MU-MIMO, Target Wake Time) that relies on centralized network management, the hybrid coordination function is integrated with the MAC layer design of 802.11ax [61]. Therefore, the CSMA/CA based throughput estimation model must be extended to support protocols (e.g., EDCA TXOP) defined with hybrid coordination. 802.11ax AP is usually equipped with high-end CPU to support the increased complexity of baseband signal processing. This provides an opportunity for WINAS to parallelize the throughput estimation, which may lead to accelerated antenna searching time by $64\times$ reduction.

Mutual coupling. The mutual coupling effect happens due to the mutual excitation of overlapped radiation field between adjacent antennas, and would result in high signal correlation. To investigate how mutual coupling may impact the throughput gained in WINAS, we conduct an experiment by increasing the space between adjacent antennas from 1cm to 30cm. The results indicate that the maximum throughput provided by the extended antenna array increases from 88 Mbps to 110 Mbps with the antenna spacing increases from 1cm to 7cm (half of the carrier wave wavelength), and does not increase when we further separate from 7cm to 30cm. The results conform with the theory that the mutual coupling effect can be avoided with antenna separation larger than half of the signal wavelength. The experimental setting follows our observation and sets the antenna spacing to 7cm.

7 Conclusion

WINAS is a general antenna augmentation system for commercial Wi-Fi APs to exploit spatial diversity gain, which is in addition to existing efforts of MIMO or beamforming. The design of WINAS addresses fundamental challenges on antenna scalability, adaptability to channel variation, and protocol compatibility, and thus makes it a general solution to standard 802.11n/ac devices. The performance of WINAS is corroborated with separate evaluation on the three main design blocks, and our real world experiments reveals up to 1.56x throughput improvement under multi-client scenario. Future works include embedding WINAS into 802.11ac beamforming operations once the CSI extraction is enabled. It will also be interesting to study how 802.11ac MU-MIMO MAC design can be adapted with slight modifications to best exploiting the performance of WINAS.

Acknowledgments

This work was supported by Alibaba Group through Alibaba Innovative Research (AIR) Program and Alibaba-NTU

Singapore Joint Research Institute (JRI) and Singapore MOE AcRF Tier 2 MOE-T2EP20220-0004. Any opinions, findings and conclusions or recommendations expressed in this material are those of the authors and do not reflect the views of Alibaba Group and other funding agencies.

REFERENCES

[1] *IEEE 802.11-2016, Part 11: Wireless LAN medium access control (MAC) and physical Layer (PHY) specifications*, 2016.

[2] V. Shrivastava, S. Rayanchu, J. Yoonj, and S. Banerjee, "11 n under the microscope," in *Proceedings of the 8th ACM SIGCOMM conference on Internet measurement*, 2008, pp. 105–110.

[3] D. Munaretto, D. Jurca, and J. Widmer, "A fast rate-adaptation algorithm for robust wireless scalable streaming applications," in *2009 IEEE International Conference on Wireless and Mobile Computing, Networking and Communications*. IEEE, 2009, pp. 246–251.

[4] W.-L. Shen, K. C.-J. Lin, S. Gollakota, and M.-S. Chen, "Rate adaptation for 802.11 multiuser mimo networks," *IEEE Transactions on Mobile Computing*, vol. 13, no. 1, pp. 35–47, 2013.

[5] M.-D. Dianu, J. Riihijärvi, and M. Petrova, "Measurement-based study of the performance of ieee 802.11 ac in an indoor environment," in *2014 IEEE International Conference on Communications (ICC)*. IEEE, 2014, pp. 5771–5776.

[6] H. Choi, T. Gong, J. Kim, J. Shin, and S.-J. Lee, "Use mu-mimo at your own risk—why we don't get gb/s wi-fi," *Ad Hoc Networks*, vol. 83, pp. 78–90, 2019.

[7] A. Goldsmith, *Wireless communications*. Cambridge university press, 2005.

[8] N. Shariati, E. Björnson, M. Bengtsson, and M. Debbah, "Low-complexity channel estimation in large-scale mimo using polynomial expansion," in *2013 IEEE 24th Annual International Symposium on Personal, Indoor, and Mobile Radio Communications (PIMRC)*. IEEE, 2013, pp. 1157–1162.

[9] O. Edfors, M. Sandell, J.-J. Van de Beek, S. K. Wilson, and P. O. Borjesson, "Ofdm channel estimation by singular value decomposition," *IEEE Transactions on communications*, vol. 46, no. 7, pp. 931–939, 1998.

[10] C. R. Athaudage and A. Jayalath, "Low-complexity channel estimation for wireless ofdm systems," in *14th IEEE Proceedings on Personal, Indoor and Mobile Radio Communications, 2003. PIMRC 2003.*, vol. 1. IEEE, 2003, pp. 521–525.

[11] Y. Gong and K. B. Letaief, "Low complexity channel estimation for space-time coded wideband ofdm systems," *IEEE Transactions on Wireless Communications*, vol. 2, no. 5, pp. 876–882, 2003.

[12] (2020) Qt7810x rf transceiver. [Online]. Available: https://www.onsemi.com/products/connectivity/wifi-solutions/qcs-ax/qt7810x

[13] I. Bahceci, T. M. Duman, and Y. Altunbasak, "Antenna selection for multiple-antenna transmission systems: Performance analysis and code construction," *IEEE Transactions on Information Theory*, vol. 49, no. 10, pp. 2669–2681, 2003.

[14] A. Gorokhov, D. A. Gore, and A. J. Paulraj, "Receive antenna selection for mimo spatial multiplexing: theory and algorithms," *IEEE Transactions on signal processing*, vol. 51, no. 11, pp. 2796–2807, 2003.

[15] A. F. Molisch and M. Z. Win, "Mimo systems with antenna selection," *IEEE microwave magazine*, vol. 5, no. 1, pp. 46–56, 2004.

[16] Z. Xu, S. Sfar, and R. S. Blum, "Analysis of mimo systems with receive antenna selection in spatially correlated rayleigh fading channels," *IEEE Transactions on Vehicular Technology*, vol. 58, no. 1, pp. 251–262, 2008.

[17] R. Nabar, "Optimal selection and use of transmit antennas in wireless systems in wireless systems," in *Proc. International Conference Telecommunication (ICT) Acapulco, Mexico, May 2000*, 2000.

[18] M. Gharavi-Alkhansari and A. B. Gershman, "Fast antenna subset selection in mimo systems," *IEEE transactions on signal processing*, vol. 52, no. 2, pp. 339–347, 2004.

[19] A. Gorokhov, "Antenna selection algorithms for mea transmission systems," in *2002 IEEE International Conference on Acoustics, Speech, and Signal Processing*, vol. 3. IEEE, 2002, pp. III–2857.

[20] I. Berenguer, X. Wang, and V. Krishnamurthy, "Adaptive mimo antenna selection via discrete stochastic optimization," *IEEE Transactions on Signal Processing*, vol. 53, no. 11, pp. 4315–4329, 2005.

[21] S. Sanayei and A. Nosratinia, "Antenna selection in mimo systems," *IEEE Communications magazine*, vol. 42, no. 10, pp. 68–73, 2004.

[22] "Huawei WLAN Smart Antenna Technology White Paper," Huawei, White Paper, 2019.

[23] S. Yoo, S. Kim, Y. Son, J. Yi, and S. Choi, "Practical antenna selection for wlan ap," in *IEEE INFOCOM 2016-The 35th Annual IEEE International Conference on Computer Communications*. IEEE, 2016, pp. 1–9.

[24] G. G. Raleigh and J. M. Cioffi, "Spatio-temporal coding for wireless communication," *IEEE Transactions on communications*, vol. 46, no. 3, pp. 357–366, 1998.

[25] C. Shepard, A. Javed, and L. Zhong, "Control channel design for many-antenna mu-mimo," in *Proceedings of the 21st Annual International Conference on Mobile Computing and Networking*, 2015, pp. 578–591.

[26] D. Bharadia and S. Katti, "Full duplex {MIMO} radios," in *11th {USENIX} Symposium on Networked Systems Design and Implementation ({NSDI} 14)*, 2014, pp. 359–372.

[27] C. Zhao, Z. Li, T. Liu, H. Ding, J. Han, W. Xi, and R. Gui, "Rf-mehndi: A fingertip profiled rf identifier," in *IEEE INFOCOM 2019-IEEE Conference on Computer Communications*. IEEE, 2019, pp. 1513–1521.

[28] T. L. Marzetta, *Fundamentals of massive MIMO*. Cambridge University Press, 2016.

[29] E. Everett, C. Shepard, L. Zhong, and A. Sabharwal, "Softnull: Many-antenna full-duplex wireless via digital beamforming," *IEEE Transactions on Wireless Communications*, vol. 15, no. 12, pp. 8077–8092, 2016.

[30] C. W. Shepard, R. Doost-Mohammady, R. E. Guerra, and L. Zhong, "Argosv3: An efficient many-antenna platform," in *Proceedings of the 23rd Annual International Conference on Mobile Computing and Networking*, 2017, pp. 501–503.

[31] A. F. Molisch, M. Z. Win, Y.-S. Choi, and J. H. Winters, "Capacity of mimo systems with antenna selection," *IEEE Transactions on Wireless Communications*, vol. 4, no. 4, pp. 1759–1772, 2005.

[32] Y. Xie, Y. Zhang, J. C. Liando, and M. Li, "Swan: Stitched wi-fi antennas," in *Proceedings of the 24th Annual International Conference on Mobile Computing and Networking*. ACM, 2018, pp. 51–66.

[33] R. G. Vaughan and J. B. Andersen, "Antenna diversity in mobile communications," *IEEE Transactions on vehicular technology*, vol. 36, no. 4, pp. 149–172, 1987.

[34] J. H. Winters, J. Salz, and R. D. Gitlin, "The impact of antenna diversity on the capacity of wireless communication systems," *IEEE transactions on Communications*, vol. 42, no. 234, pp. 1740–1751, 1994.

[35] D. A. Gore and A. J. Paulraj, "Mimo antenna subset selection with space-time coding," *IEEE Transactions on signal processing*, vol. 50, no. 10, pp. 2580–2588, 2002.

[36] R. W. Heath and A. Paulraj, "Antenna selection for spatial multiplexing systems based on minimum error rate," in *ICC 2001. IEEE International Conference on Communications. Conference Record (Cat. No. 01CH37240)*, vol. 7. IEEE, 2001, pp. 2276–2280.

[37] A. Yılmaz and O. Kucur, "Performances of transmit antenna selection, receive antenna selection, and maximal-ratio-combining-based hybrid techniques in the presence of feedback errors," *IEEE Transactions on vehicular technology*, vol. 63, no. 4, pp. 1976–1982, 2013.

[38] T. Eriksson and T. Ottosson, "Compression of feedback for adaptive transmission and scheduling," *Proceedings of the IEEE*, vol. 95, no. 12, pp. 2314–2321, 2007.

[39] A. Dhekne, M. Gowda, R. R. Choudhury, and S. Nelakuditi, "If wifi aps could move: A measurement study," *IEEE Transactions on Mobile Computing*, vol. 17, no. 10, pp. 2293–2306, 2018.

[40] J. Xiong, K. Sundaresan, K. Jamieson, M. A. Khojastepour, and S. Rangarajan, "Midas: Empowering 802.11 ac networks with multiple-input distributed antenna systems," in *Proceedings of the 10th ACM International on Conference on emerging Networking Experiments and Technologies*, 2014, pp. 29–40.

[41] Z. Li, Y. Xie, L. Shangguan, R. I. Zelaya, J. Gummeson, W. Hu, and K. Jamieson, "Towards programming the radio environment with large arrays of inexpensive antennas," in *16th {USENIX} Symposium on Networked Systems Design and Implementation ({NSDI} 19)*, 2019, pp. 285–300.

[42] H. S. Rahul, S. Kumar, and D. Katabi, "Jmb: scaling wireless capacity with user demands," *ACM SIGCOMM Computer Communication Review*, vol. 42, no. 4, pp. 235–246, 2012.

[43] E. Perahia and R. Stacey, *Transmit beamforming*. Cambridge University Press, 2008, p. 305–306.

[44] A. Gupta, J. Min, and I. Rhee, "Wifox: Scaling wifi performance for large audience environments," in *Proceedings of the 8th international conference on Emerging networking experiments and technologies*, 2012, pp. 217–228.

[45] A. Mcgregor and D. Smithies, "Rate adaptation for 802.11 wireless networks: Minstrel," *Submitted to ACM SIGCOMM*, 2010.

[46] M. Mirza, P. Barford, X. Zhu, S. Banerjee, and M. Blodgett, "Fingerprinting 802.11 rate adaption algorithms," in *2011 Proceedings IEEE INFOCOM*. IEEE, 2011, pp. 1161–1169.

[47] Y. Xie, Z. Li, and M. Li, "Precise power delay profiling with commodity wifi," in *Proceedings of the 21st Annual International Conference on Mobile Computing and Networking*, ser. MobiCom '15. New York, NY, USA: ACM, 2015, p. 53–64. [Online]. Available: http://doi.acm.org/10.1145/2789168.2790124

[48] M. Schulz, J. Link, F. Gringoli, and M. Hollick, "Shadow wi-fi: Teaching smartphones to transmit raw signals and to extract channel state information to implement practical covert channels over wi-fi," in *Proceedings of the 16th Annual International Conference on Mobile Systems, Applications, and Services*, ser. MobiSys '18. New York, NY, USA: Association for Computing Machinery, 2018, p. 256–268. [Online]. Available: https://doi.org/10.1145/3210240.3210333

[49] COMPEX, *WPJ558*, 2018 (accessed Feb. 4, 2020). [Online]. Available: https://compex.com.sg/shop/embedded-board/wpj558-2/

[50] B. G. Lee and S. Choi, *Broadband wireless access and local networks: mobile WiMAX and WiFi*. Artech House, 2008.

[51] D. Tse and P. Viswanath, *Fundamentals of wireless communication*. Cambridge university press, 2005.

[52] H. Assasa and J. Widmer, "Implementation and evaluation of a wlan ieee 802.11 ad model in ns-3," in *Proceedings of the Workshop on Ns-3*, 2016, pp. 57–64.

[53] D. Halperin, W. Hu, A. Sheth, and D. Wetherall, "Predictable 802.11 packet delivery from wireless channel measurements," *ACM SIGCOMM Computer Communication Review*, vol. 41, no. 4, pp. 159–170, 2011.

[54] ——, "Tool release: Gathering 802.11n traces with channel state information," *ACM SIGCOMM CCR*, vol. 41, no. 1, p. 53, Jan. 2011.

[55] G. Pei and T. R. Henderson, "Validation of ofdm error rate model in ns-3," 2010.

[56] A. Langley, A. Riddoch, A. Wilk, A. Vicente, C. Krasic, D. Zhang, F. Yang, F. Kouranov, I. Swett, J. Iyengar *et al.*, "The quic transport protocol: Design and internet-scale deployment," in *Proceedings of the Conference of the ACM Special Interest Group on Data Communication*, 2017, pp. 183–196.

[57] M. Youssef and A. Agrawala, "The horus wlan location determination system," in *Proceedings of the 3rd international conference on Mobile systems, applications, and services*, 2005, pp. 205–218.

[58] H. Zhang, A. F. Molisch, and J. Zhang, "Applying antenna selection in wlans for achieving broadband multimedia communications," *IEEE Transactions on Broadcasting*, vol. 52, no. 4, pp. 475–482, 2006.

[59] V. Erceg, "Ieee p802. 11 wireless lans tgn channel models," *IEEE 802.11-03/940r4*, 2004.

[60] G. Tan and J. V. Guttag, "Time-based fairness improves performance in multi-rate wlans." in *USENIX annual technical conference, general track*, 2004, pp. 269–282.

[61] E. Khorov, A. Kiryanov, A. Lyakhov, and G. Bianchi, "A tutorial on ieee 802.11 ax high efficiency wlans," *IEEE Communications Surveys & Tutorials*, vol. 21, no. 1, pp. 197–216, 2018.

Yanbo Zhang receives the B.E. degree in communication from Harbin Institute of Technology, Harbin, China in 2017. He is currently working toward the PhD degree in computer science and engineering at Nanyang Technological University. His research interests include wireless communication and sensing systems, internet of things and mobile computing.

Weiping Sun received his B.S. degree in network engineering from Dalian University of Technology, Dalian, China, in 2006, and his Ph.D. degree in electrical engineering from Seoul National University, Seoul, South Korea, in 2017. He had worked as a postdoc research fellow in Nanyang Technological University, Singapore, from 2018 to 2020. He joined Samsung Research, Seoul, South Korea, in 2020, where he is a staff engineer, working on the next generation cellular system. His research interests include RF-based sensing, PHY/MAC designs of cellular networks, WLAN, WPAN, and coexistence among heterogeneous networks.

Yidong Ren received the BE degree in electrical and information engineering from University of Electronic Science and Technology of China, Chengdu, China. He is currently working toward the PhD degree in the Department of Computer Science and Engineering, Michigan State University, USA. His primary research interests include wireless networks, mobile computing and IoT system.

Sung-Ju Lee is a Professor and KAIST Endowed Chair Professor at KAIST. He received his Ph.D. in computer science from the University of California, Los Angeles in 2000, and spent 15 years in the industry in Silicon Valley before joining KAIST. His research interests include computer networks, mobile computing, network security, and HCI. He is the winner of the HP CEO Innovation Award, the Best Paper Award at IEEE ICDCS 2016, and the Test-of-Time Paper Award at ACM WINTECH 2016. He is an IEEE Fellow and ACM Distinguished Scientist.

Mo Li (M'06) received the B.S. degree in computer science and technology from Tsinghua University, Beijing, China, in 2004, and the Ph.D. degree in computer science and engineering from The Hong Kong University of Science and Technology, Hong Kong, in 2009. He is currently an Associate Professor with the School of Computer Science and Engineering, Nanyang Technological University, Singapore. His research interests include networked and distributed sensing, wireless and mobile, cyber-physical systems, smart city, and urban computing.